Journal of Materials Chemistry C

ROYAL SOCIETY OF CHEMISTRY

PAPER

View Article Online
View Journal | View Issue

Cite this: J. Mater. Chem. C, 2023, 11, 10893

Enabling red thermally activated delayed fluorescence by increasing the push–pull strength in naphthalimide-phenothiazine derivatives†

Chiara Montanari,‡[a] Tommaso Bianconi, ‡[a] Manju Sheokand,‡[b] Titouan Teunens, [cd] Giulia Cavalletti,[a] Jérôme Cornil, [d] Rajneesh Misra *[b] and Benedetta Carlotti *[a]

In this study, we report the synthesis of a series of six new push–pull compounds, bearing naphthalimide as the electron acceptor and phenothiazine or phenothiazine dioxide as the electron donor, arranged in dipolar or octupolar molecular structures and showing either a single bond or a phenyl spacer as the linker between units. This synthetic effort allowed a detailed investigation of the structure–property relationships and of the key factors enabling thermally activated delayed fluorescence (TADF) in these fluorophores, performed through a joint advanced time-resolved spectroscopic and TD-DFT computational approach. Our ultrafast spectroscopic results showed larger push–pull degree for the phenothiazine compared to the phenothiazine dioxide derivatives. This resulted in negligible energy gap between the intramolecular charge transfer S_1 and the naphthalimide localized T_1 excited states, and thus lead to effective reverse intersystem crossing and TADF only in the case of the oxygen-free compounds. The increased conjugation in the octupolar relative to the dipolar systems as well as in the phenyl-bridged structures allowed higher fluorescence efficiencies to be achieved. The red TADF of these luminophores, less common and more difficult to achieve than blue and green TADF, was found to be enhanced in their aggregates produced both in water dispersions and in thin films. The observation of intense red TADF in the solid state makes these new all-organic materials highly promising for applications in third generation OLED devices.

Received 4th June 2023,
Accepted 26th June 2023

DOI: 10.1039/d3tc01939j

rsc.li/materials-c

Introduction

Organic light emitting diodes (OLEDs) utilizing thermally activated delayed fluorescence (TADF) active materials have attracted tremendous attention lately, more than fluorescence- and phosphorescence-based devices.[1–4] In fact, according to spin statistics, electrogenerated singlet and triplet excitons are obtained in 1 : 3 ratio. Therefore, conventional fluorescent OLEDs are limited to a maximum internal quantum efficiency of 25%. On the other hand, the more efficient phosphorescent OLEDs generally employ rare noble metal complexes (*e.g.* Ir and Pt) with several obvious drawbacks, such as high costs and toxicity due to heavy atoms and the absence of stable blue emitters.[5,6] TADF-based OLEDs, characterized by potential 100% internal quantum efficiencies and all-organic low-cost active materials, have emerged as an alternative approach for third generation devices and have aroused great interest within the last decade.

According to the El-Sayed rules, significant spin orbit coupling (SOC) in all-organic chromophores may be obtained if singlet and triplet excited states of different orbital nature are involved in the intersystem crossing (ISC). Intramolecular charge transfer interactions in molecular systems bearing electron donating and electron accepting units can not only promote SOC and hence efficient ISC but also lower the energy difference between the lowest singlet and triplet excited states.[7–10] A small singlet-to triplet energy splitting (ΔE_{ST}), defined as the gap between the T_1 and S_1 states, is the most important criterion to achieve relatively high rates of reverse intersystem crossing (r-ISC)

[a] Department of Chemistry, Biology and Biotechnology and CEMIN, University of Perugia, via Elce di sotto n.8, 06123 Perugia, Italy. E-mail: benedetta.carlotti@unipg.it
[b] Department of Chemistry, Indian Institute of Technology, Indore 453552, India. E-mail: rajneeshmisra@iiti.ac.in
[c] Laboratoire de Chimie Organique et Photochimie, Université Libre de Bruxelles, 50 avenue Franklin D. Roosevelt, CP 160/08, 1050 Bruxelles, Belgium
[d] Service de Chimie des Matériaux Nouveaux, Université de Mons, 20 place du Parc, 7000 Mons, Belgium

† Electronic supplementary information (ESI) available: Experimental section; absorption and emission properties; ultrafast spectroscopy; triplet properties; excited state energy and nature; thermally activated delayed fluorescence; aggregation induced and solid state delayed fluorescence; quantum chemical simulations. See DOI: https://doi.org/10.1039/d3tc01939j

‡ Equally contributed as first authors.

followed by significant delayed fluorescence. It is generally recognized that $\Delta E_{ST} < 0.2$eV is necessary for competitive r-ISC and TADF.[11]

While many efficient blue and green TADF materials have been developed by suitably connecting donor and acceptor portions,[5,12–14] there are currently few examples of orange-red and infrared TADF materials.[15–21] Thus, an efficient molecular design strategy is required to boost the efficiency of red TADF materials. Indeed, red materials possess smaller bandgap than blue and green TADF materials. This leads to the nonradiative decay of the S_1 excitons to be generally predominant in the red region due to the energy gap law. Additionally, the strong donor–acceptor character of the employed TADF fluorophores, whose excited state charge rearrangement may also be accompanied by twisting of the molecular structure, often leads to low efficiency of the radiative deactivation. An effective strategy to reduce the competition of internal conversion and vibrational relaxation processes may be to introduce more rigid and more conjugated molecular structures. On the other hand, materials with the integration of aggregation-induced emission (AIE) and TADF properties can not only effectively suppress the nonradiative pathways by restriction of intramolecular motions but also reduce the quenching of the triplet state by molecular oxygen as the aggregates may prevent the interaction.[2,22] Many AIE-TADF emitters have been reported to show good performance in non-doped OLEDs.[23–26]

Recently, our research has been devoted to the study of several push–pull phenothiazine derivatives for their photoinduced intramolecular charge transfer (ICT) ability and nonlinear optical properties.[27–30] Interestingly, phenothiazine has been described in literature reports as a remarkable electron donor unit for the development of orange/red TADF luminogens.[22,31–33] To this aim, we have here considered a comprehensive series of six donor–acceptor compounds (Chart S1, Scheme 1, ESI†) where the electron donor portion is phenothiazine (PTZ) or phenothiazine dioxide (PTZ(dioxy)) and the electron acceptor is naphthalimide (NPI). The donor and acceptor units were simply connected through a single bond (A–D: **NPI-PTZ** and **NPI-PTZ(dioxy)**) or through a phenyl π-bridge (A–Ph–D: **NPI-Ph-PTZ** and **NPI-Ph-PTZ(dioxy)**) in dipolar structures with lower and higher conjugation, respectively. Additionally, the molecular conjugation was also enhanced by arranging the donor and acceptor units in octupolar structures of A_3–D kind (**NPI(3)-PTZ** and **NPI(3)-PTZ(dioxy)**). The present study wants to get a deep insight into the structure-TADF property relationships by a joint synthetic, spectroscopic and computational effort. State-of-the-art time resolved spectroscopies with both nanosecond and femtosecond temporal resolution, both in absorption and emission, have been employed to follow the triplet and singlet excited state dynamics of the newly synthetized compounds. Furthermore, information about the excited state energy and nature was gained by means of advanced TD-DFT calculations. The photophysics of these new fluorophores was investigated for the monomers in solution as well for the aggregates produced both in water dispersion and in the solid state.

Results and discussion

Synthesis

The synthetic procedure for the phenothiazine and phenothiazine sulfone derivatives incorporated with 1,8-napthalimide are shown in Scheme 1. The **NPI-PTZ** chromophore was synthesized by the Buchwald–Hartwig cross-coupling reaction of 10*H*-phenothiazine with one equivalent of 6-bromo-2-(2-ethylhexyl)-1*H*-benzo[de]isoquinoline-1,3(2*H*)-dione NPI-Br in the presence of $Pd(OAc)_2$ as the catalyst and $P(^tBu)_3HBF_4$ as a ligand in 84% yield (Scheme 1). The chromophore **NPI-PTZ** was further reacted with 3 equiv. of 3-chloroperbenzoic acid in dichloromethane solution which resulted **NPI-PTZ(dioxy)** in 87% yield. The phenyl spacer containing **NPI-Ph-PTZ** was synthesized *via* the Pd-catalysed Suzuki cross-coupling of 6-bromo-2-(2-ethylhexyl)-1*H*-benzo[de]isoquinoline-1,3(2*H*)-dione NPI-Br with one equivalent of 10-(4-(4,4,5,5-tetramethyl-1,3,2-dioxaborolan-2-yl)phenyl)-10*H*-phenothiazine PTZ-BP in 63% yield (Scheme 1). **NPI-Ph-PTZ** was further oxidized using three equivalents of 3-chloroperbenzoic acid in dichloromethane and resulted **NPI-Ph-PTZ(dioxy)** in 87% yield (Scheme 1). The star-shaped tri-1,8-napthalimde units functionalized chromophore **NPI(3)-PTZ** was synthesized by reacting the 6-(3,7-dibromo-10H-phenothiazin-10-yl)-2-(2-ethylhexyl)-1*H*-benzo[de]isoquinoline-1,3(2*H*)-dione 1 with 2-(2-ethylhexyl)-6-(4,4,5,5-tetramethyl-1,3,2-dioxaborolan-2-yl)-1*H*-benzo[de]isoquinoline-1,3(2*H*)-dione 2 through the Suzuki cross-coupling reaction in 75% yield (Scheme 1). The detailed synthetic procedure of intermediates 1 and 2 is given in the ESI.† The oxidized sulfone derivative **NPI(3)-PTZ(dioxy)** was further synthesized from **NPI(3)-PTZ** by following the oxidation procedure and resulted in 88% yield (Scheme 1).

Absorption and emission properties

Fig. 1 shows the normalized absorption and emission spectra of the six investigated compounds in toluene. The absorption spectra (Fig. 1A) are composed by a main structured band centered at 335–355 nm depending on the molecular structure, and in most cases by a less intense bathochromic shoulder between 370 and 450 nm. The main absorption band exhibits a clear red-shift by increasing the molecular conjugation among the compounds in the series. Indeed, it is centered at 336 nm for the dipolar systems where the donor and acceptor units are connected by single bonds (D–A); it is slightly shifted toward longer wavelengths for the dipolar systems where the bridge is a phenyl ring (D–Ph–A); it is even more red-shifted for the two octupolar compounds ($D–A_3$). The DFT computational study in toluene allowed a deep understanding of the nature of the observed absorption transitions. Fig. 2 reports the results obtained for the representative case of **NPI-PTZ(dioxy)**. The main absorption band corresponds to the $S_0 \rightarrow S_2$ transition with large oscillator strength and described by hole and electron natural transition orbitals (NTOs) localized on the naphthalimide. The bathochromic shoulder is due to the forbidden $S_0 \rightarrow S_1$ described by a HOMO–LUMO transition, with the HOMO localized on the phenothiazine dioxide donor and

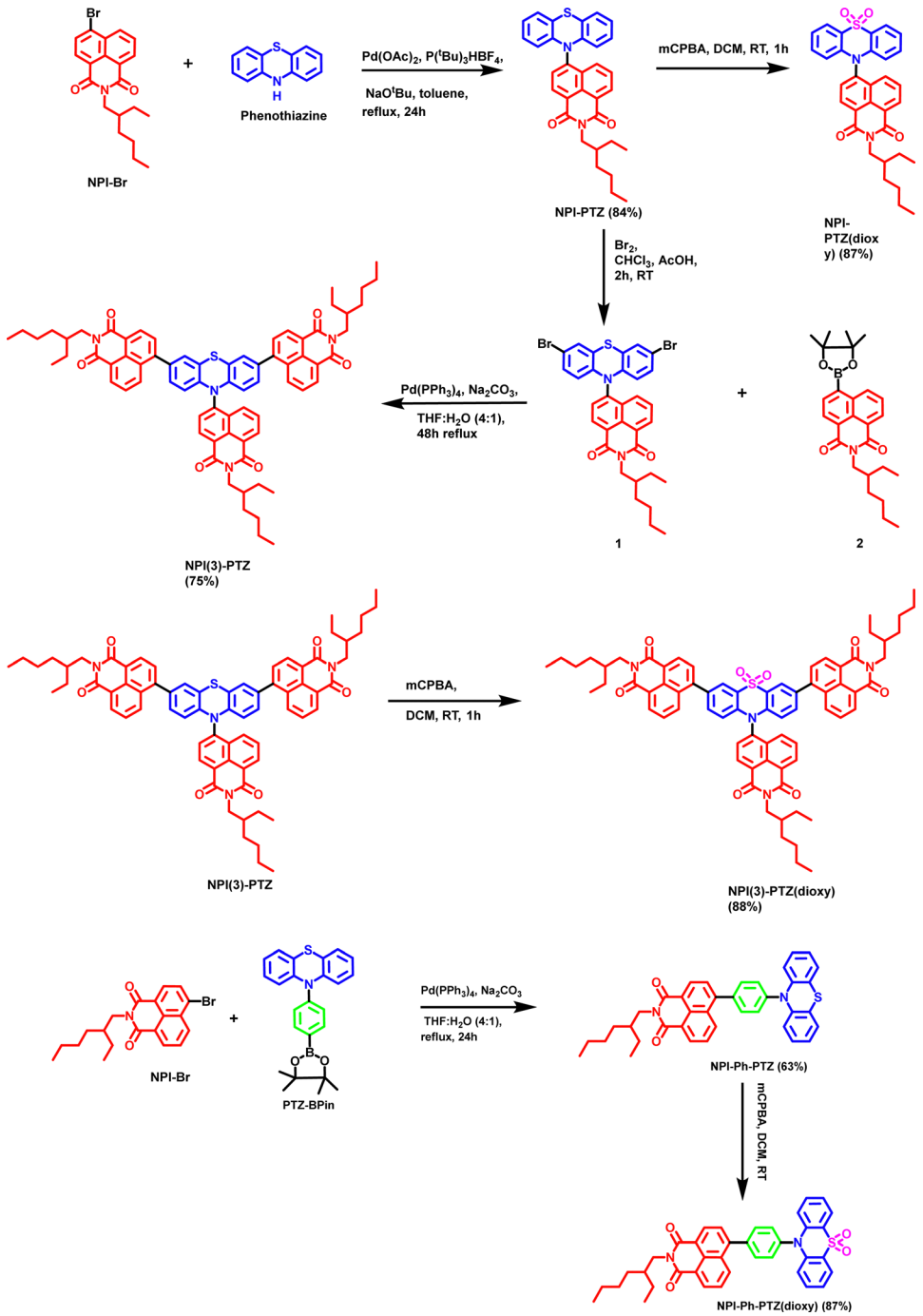

Scheme 1 Synthetic route to obtain **NPI-PTZ**, **NPI-PTZ(dioxy)**, **NPI(3)-PTZ**, **NPI(3)-PTZ(dioxy)**, **NPI-Ph-PTZ** and **NPI-Ph-PTZ(dioxy)**.

the LUMO on the naphthalimide acceptor, thus with a clear charge transfer character. Similar findings for all the other compounds are detailed in the ESI.† The $S_0 \rightarrow S_1$ transition is found at lower energies for the phenothiazine derivatives (*e.g. ca.* 450 nm for **NPI-PTZ**, *ca.* 400 nm for **NPI-Ph-PTZ**, *ca.* 430 nm for **NPI(3)-PTZ**) relative to the phenothiazine dioxide analogues (see Table S1, ESI†). This is justified by the larger ICT degree of S_1 for the compounds bearing the stronger PTZ electron donor unit relative to PTZ(dioxy). This is demonstrated by the DFT simulations considering the larger charge density of the HOMO localized on the electron donor phenothiazine unit compared to that on the phenothiazine dioxide (see Fig. S40, ESI†).

This computational result gives also a justification to the significant differences among the emission spectra of the six compounds (Fig. 1B). All the investigated molecules show a broad non-structured emission in toluene. The phenothiazine derivatives exhibit significantly red-shifted spectra relative to the phenothiazine dioxide analogues, particularly **NPI-PTZ** and **NPI(3)-PTZ**, in agreement with an enhanced ICT character of their lowest excited singlet state. A peculiar behavior was

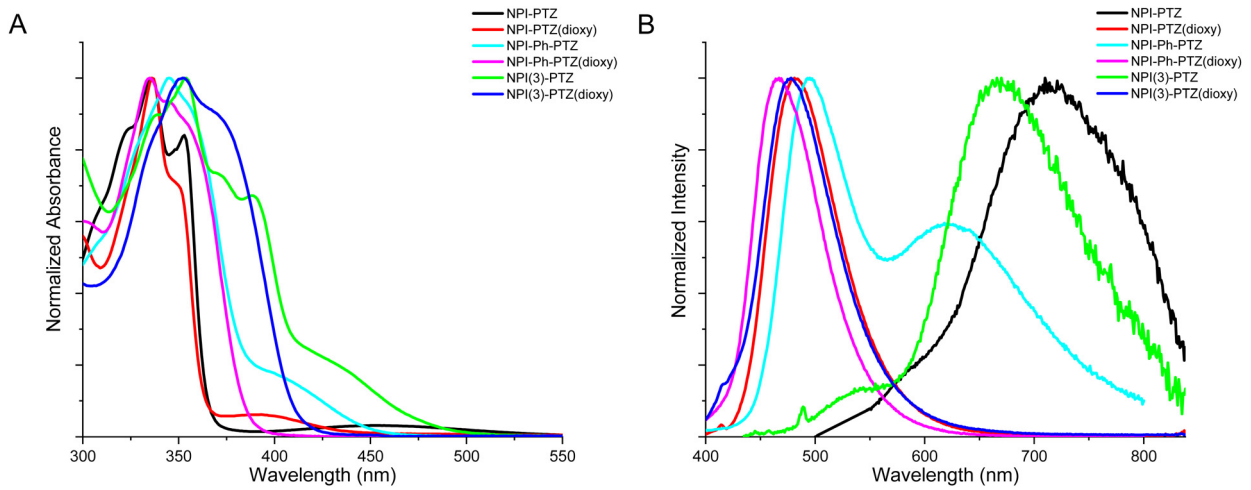

Fig. 1 Normalized absorption (A) and fluorescence (B) spectra of the investigated compounds in toluene (emission spectra were generally recorded by exciting at the lowest energetic shoulder of the absorption spectrum, with the exception of **NPI-Ph-PTZ(dioxy)** for which a 335 nm excitation was used).

revealed for the case of **NPI-Ph-PTZ**, for which two emission bands were detected in toluene (Fig. 1B). The reasons underlying this peculiarity were further investigated through the study of the solvent effect on the spectra. For all the investigated samples, a small solvatochromism was observed on the absorption spectra: just a small red-shift on passing from the methylcyclohexane/3-methylpentane mixture to toluene and from toluene to dimethylsulphoxide (Fig. S18 and S20, ESI†). On the other hand, a large solvent effect was observed on the emission spectra, that show a significant positive fluorosolvatochromism upon increasing the solvent polarity (Fig. S19 and S20, ESI†). In the case of **NPI-Ph-PTZ**, the emission spectrum significantly red-shifts in the more polar solvents, with a noticeable dual emission clearly exhibited in toluene but also hinted in dimethylsulphoxide. This behavior, typical of push–pull systems,[34–38] can be rationalized considering the progressive stabilization of an intramolecular charge transfer (ICT) excited state with increasing the solvent polarity as well as the presence of two relative minima on the potential energy curve of S_1, that are the locally excited (LE) state populated by light absorption and the fully relaxed ICT state.

In Table 1, the fluorescence quantum yields (ϕ_F), lifetimes (τ_F) and rate constants ($k_F = \phi_F/\tau_F$) are reported for the six fluorophores in toluene. The ϕ_F values are generally quite low, suggesting that non-radiative pathways may be important for the S_1 deactivation of these molecules. The fluorescence efficiency is increased on passing from the phenothiazine to the phenothiazine dioxide derivatives. Moreover, a small enhancement of the radiative quantum yields and rate constants is observed on passing from the dipolar to the octupolar systems and a large enhancement by adding a phenyl bridge between the donor and the acceptor units. This finding is in agreement with the relatively more intense bathochromic shoulder observed in the absorption spectra of the octupolar and phenyl-linked derivatives (Fig. 1A), thus revealing an increased oscillator strength for the S_0–S_1 transition for the more conjugated compounds both in absorption and in emission. The fluorescence quantum yield is decreased while the fluorescence

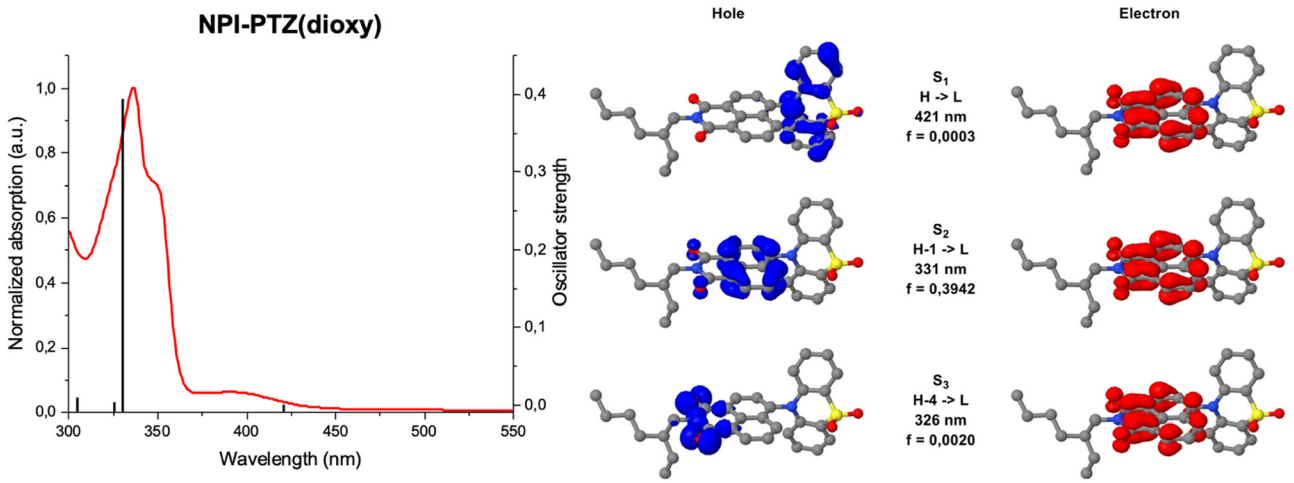

Fig. 2 Analysis of the absorption transitions for the representative case of **NPI-PTZ(dioxy)**.

Table 1 Fluorescence properties of the investigated compounds in toluene

Compound	ϕ_F	τ_{S1} (ns)	k_F (s^{-1})
NPI-PTZ	0.0015	2.5	5.9×10^5
NPI-PTZ(dioxy)	0.010	6.0	1.7×10^6
NPI-Ph-PTZ	0.076	9.7	7.8×10^6
NPI-Ph-PTZ(dioxy)	0.81	2.9	2.8×10^8
NPI(3)-PTZ	0.009	7.0	1.3×10^6
NPI(3)-PTZ(dioxy)	0.040	7.0	5.7×10^6

lifetime is generally found to be longer upon increasing the solvent polarity, with a consequent drop of the k_F in the more polar solvents (Table S1, ESI†). This is a typical behavior for donor–acceptor fluorophores due to a strong competition of the ICT leading to fluorescence quenching in the most polar media.[39,40]

Ultrafast spectroscopy

The excited state dynamics of these compounds was investigated by ultrafast spectroscopy, both in absorption and in emission, through femtosecond transient absorption (TA) and broadband fluorescence up conversion (FUC) measurements with a 400 nm laser excitation. Fig. 3 shows the results obtained for **NPI-Ph-PTZ** in toluene as a representative example. The TA spectra (panel B of the left graph) show a remarkable temporal evolution. The initially formed excited state absorption band (in black) exhibits a blue-shift in time after photoexcitation to give within few picoseconds another spectral shape (in green) characterized by a major peak at *ca.* 650 nm and a secondary band at *ca.* 470 nm. This transient species was found to decay in hundreds of picoseconds to give another structured excited state absorption (ESA) with two maxima at *ca.* 525 and 575 nm (in red). This signal decays on a longer time scale of few nanoseconds. The global analysis of the TA data revealed the presence of five components (panel C of the left graph): the first two with lifetimes of 0.54 and 5.0 ps were assigned to inertial and diffusive solvation in toluene (black); the third component with a lifetime of 140 ps and showing the 470 and 650 nm ESA peaks (green) to the LE S_1 state; the forth component with a lifetime of 9700 ps and the structured 525 and 575 nm ESA (red) to the ICT state; the fifth component not decaying in the investigated time window of few nanoseconds (Inf, blue) was associated to the long-lived triplet excited state T_1. Analysis of the spectral shapes of the observed transients is at the root of the LE and ICT state assignments in the TA as well as the FUC results. The broadband FUC measurements highlighted in the time-resolved emission spectra (panel B of the right graph) a small initial red-shift with time to give the main 525 nm emission band (green). This band is then found to decay and only at long delays after excitation another less intense and red-shifted emission peaked at *ca.* 650 nm becomes apparent (red). The global analysis of these data revealed the presence of four components, in good agreement with the TA: the first two components (0.28 and 4.7 ps, in black) associated to solvation; the third component (140 ps, in green) characterized by the intense 525 nm emission assigned to the LE state and the fourth component (3100 ps, in red) characterized by the low intensity 650 nm emission corresponding to the ICT state. These results allow a deep understanding of the steady-state

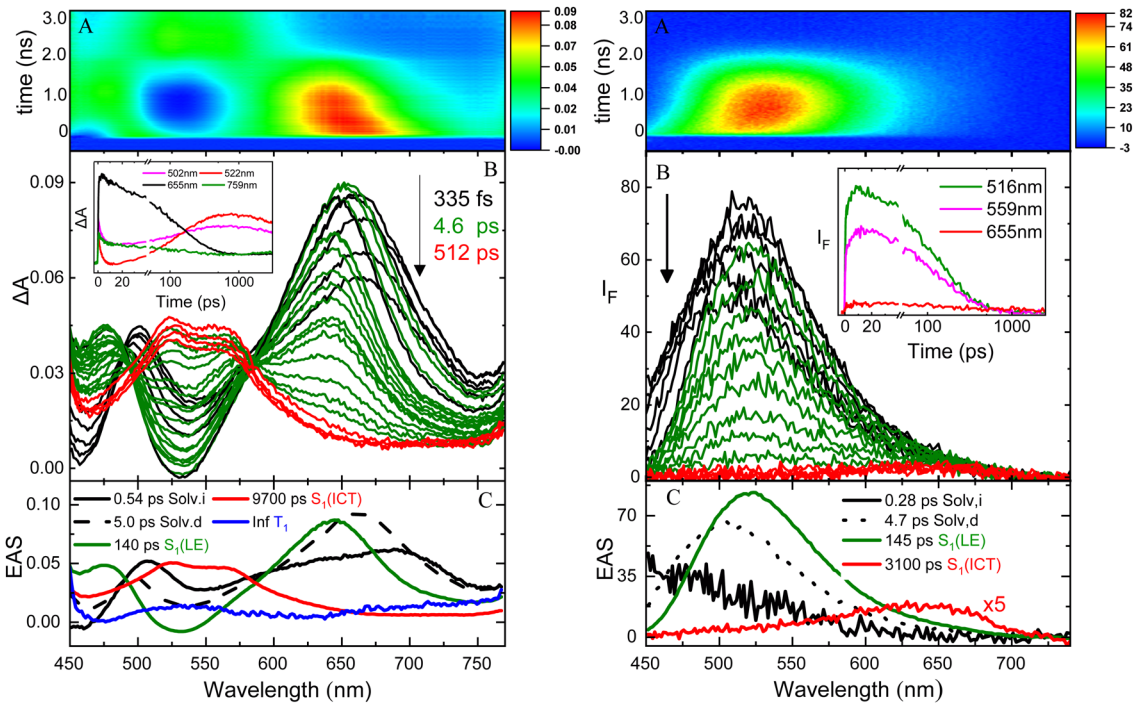

Fig. 3 Femtosecond transient absorption (left) and broadband fluorescence up conversion spectroscopy (right) of **NPI-Ph-PTZ** in toluene with a 400 nm laser excitation (panel A: $\Delta A/I_F$ *vs.* wavelength and time colored map; panel B: time resolved absorption/emission spectra and kinetics at selected wavelengths (inset); panel C: Evolution Associated Spectra (EAS) and lifetimes of the components obtained through global analysis).

Table 2 Results of global analysis of the femtosecond transient absorption data for the investigated compounds in Tol and DMSO

Solvent	τ / ps						Assignment
	NPI-PTZ	NPI-Ph-PTZ	NPI(3)-PTZ	NPI-PTZ(dioxy)	NPI-Ph-PTZ(dioxy)	NPI(3)-PTZ(dioxy)	
Tol	0.45	0.54		0.27		0.91	$Solv._i$ / S_1(LE)
		5.0	2.0	3.1	7.4		$Solv._d$
	14	140	500	170	120	130	SR
	2500	9700	7000	6000	2900	7000	S_1(ICT)
	Inf	Inf	Inf	Inf	Inf	Inf	T_1
DMSO	0.25	1.0	0.60	0.18		0.59	$Solv._i$ / S_1(LE)
	1.7	4.7		2.3	2.2	4.3	$Solv._d$
				480	340	39	SR
	9.6	27	4.0	8160	6370	7440	S_1(ICT)
				Inf		Inf	T_1

$Solv._i$ and $Solv._d$: inertial and diffusive solvation; SR: structural relaxation.

dual emission exhibited by **NPI-Ph-PTZ** in toluene as due to the LE and ICT fluorescence. For these remarkably push–pull compounds, population of the ICT from the LE state is thus observed even in a low polar solvent, such as toluene (Table 2).

The LE → ICT transition in toluene takes place in ultrashort times comparable to the solvation times for the dipolar and octupolar derivatives for which the donor and acceptor units are linked through a single bond, while occurring in hundreds of picoseconds if a phenyl is inserted as π-bridge (Table 2). Indeed, increasing the distance between the donor and acceptor units through the insertion of a phenyl bridge may lead to a decrease in the rate of the ICT process. For this reason, the LE-ICT transition in **NPI-Ph-PTZ** appears to be slower than for the analogous compounds without the phenyl bridge (Table 2). In a more polar solvent, such as dimethylsulphoxide, the LE → ICT transition happens faster, with times comparable to the inertial solvation in all cases. It is noteworthy that for the dioxy-derivatives the ICT excited state shows a long lifetime of few nanoseconds also in the highly polar medium dimethylsulphoxide. On the other hand, for the oxygen free phenothiazine derivatives, the ICT lifetime is significantly shortened in dimethylsulphoxide, being few picoseconds for **NPI-PTZ** and **NPI(3)-PTZ** and tens of picoseconds for **NPI-Ph-PTZ**. This finding suggests a preferential ultrafast deactivation by internal conversion for the exceptionally stabilized ICT states of the oxygen-free phenothiazine derivatives. It is possible that population of the ICT state is accompanied by rotation around the quasi-single bonds between the donor and acceptor units in the more flexible oxygen-free derivatives (Twisted ICT states). On the other hand, for the more rigid oxygen-functionalized derivatives, ICT states characterized by a more planar geometry (Planar ICT states) are likely populated thus exibiting longer lifetimes even in highly polar solvents.[29]

Triplet properties

The occurrence of another non-radiative deactivation pathway, other than the ICT, such as the intersystem crossing (ISC) was investigated by means of nanosecond transient absorption measurements. Significant ESA signals were revealed for all the investigated compounds in toluene (Fig. 4 and Fig. S28, ESI†).

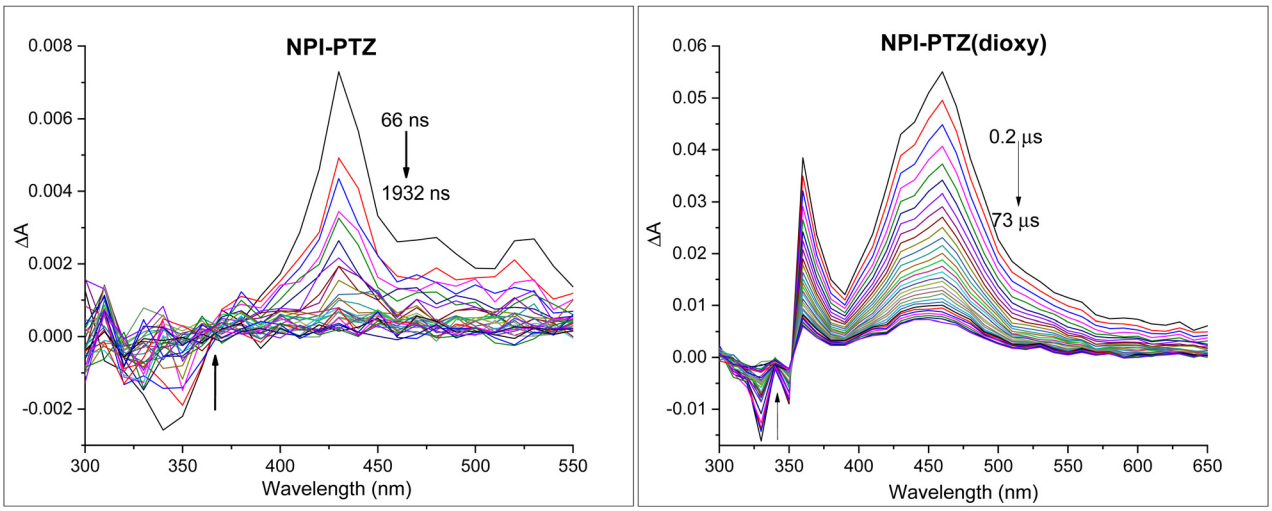

Fig. 4 Triplet absorption spectrum for **NPI-PTZ** and **NPI-PTZ(dioxy)** in nitrogen purged toluene.

Table 3 Triplet properties of the investigated compounds in toluene

Compound	λ_T (nm)	$\tau_{T,N2}$ (ns)	ε_T (M^{-1} cm^{-1})	ϕ_T
NPI-PTZ	430	6 (3%) 440 (97%)	7630[a]	0.27
NPI-PTZ(dioxy)	460	44000	7680[a]	0.88
NPI-Ph-PTZ	460	24000	3000[a]	0.61
NPI-Ph-PTZ(dioxy)	400	12000	3050[a]	0.19
NPI(3)-PTZ	660	19 (1%) 3400 (99%)	7350[b]	0.21
NPI(3)-PTZ(dioxy)	670	45000	8300[b]	0.93

[a] In acetonitrile. [b] In cyclohexane.

The TA spectra in toluene showed ESA bands peaked around 400–460 nm for the dipolar systems, while being red-shifted and centred around 660–670 nm for the octupolar derivatives (Table 3). The recorded kinetics exhibited decays significantly affected by the presence of molecular oxygen in solution for all the investigated samples (Table S3, ESI†), suggesting the triplet excited state nature of the observed transient species. The triplet lifetimes were found to be longer in the phenothiazine dioxide as compared to the phenothiazine derivatives as well as in the more conjugated molecules relative to the smallest **NPI-PTZ** compound (Table 3). A peculiar behaviour was revealed in the decay kinetics recorded for **NPI-PTZ** and **NPI(3)-PTZ**, both in air-equilibrated and nitrogen-purged toluene. The kinetics were best fitted by using a bi-exponential decay function, with a first component showing a lifetime of few nanoseconds comparable to the ns-laser pulse duration (*ca.* 7 ns) and a second component showing a lifetime of tens/hundreds of nanoseconds in aerated solution which becomes significantly longer up to few microseconds in de-aereated toluene (Fig. S29 and S30, Table 3, ESI†). This latter lifetime can be unambiguously assigned to the triplet excited state. It may be possible to suggest an efficient r-ISC process which could yield a shortly delayed fluorescence in the case of these two molecules (**NPI-PTZ** and **NPI(3)-PTZ**) to justify the presence of the first short-lived component in the TA kinetics recorded by nanosecond laser flash photolysis.

Sensitization experiments allowed triplet extinction coefficients (ε_T) between 3000 and 8000 M^{-1} cm^{-1} to be accurately determined for the investigated molecules (Table 3). Relative actinometry measurements were carried out to obtain the triplet quantum yields in toluene (ϕ_T in Table 3), which were found to be significant for all the six compounds, proving ISC as an important decay pathway for their excited states. The triplet yield values were measured to be *ca.* 20–30% for **NPI-PTZ** and **NPI(3)-PTZ**, while being enhanced up to *ca.* 90% for their dioxy-analogues. A different trend was observed for the compounds showing a phenyl as π-bridge, where a more efficient ISC was revealed for the oxygen free (61%) relative to the oxygen functionalized derivative (19%). For all the phenothiazine dioxide compounds in toluene it was found that $\phi_F + \phi_T \approx 100\%$, indicating that the fluorescence and the ISC quantitively account for the S_1 deactivation. The introduction of the phenyl bridge in **NPI-Ph-PTZ(dioxy)** has the effect of enhancing the fluorescence (81%) at the expenses of the intersystem crossing (19%) relative to the other oxygen-functionalized derivative, as expected considering the increase in conjugation. For the oxygen-free phenothiazine derivatives instead $\phi_F + \phi_T < 100\%$, particularly for the case of **NPI-PTZ** and **NPI(3)-PTZ**, suggesting that an important role is played by the ICT followed by internal conversion to the ground state for these molecules. Both the fluorescence and the intersystem crossing quantum yields are enhanced in **NPI-Ph-PTZ** relative to **NPI-PTZ** and **$(NPI)_3$-PTZ** for its reduced push–pull character due to the increased distance between the donor and acceptor units.

Excited state energy and nature

In order to investigate the possible communication between S_1 and T_1 suggested by the laser flash photolysis kinetics for **NPI-PTZ** and **NPI(3)-PTZ**, information about the energy of the lowest excited singlet and triplet states was gained through fluorescence and phosphorescence experiments in the methylcyclohexane/3-methylpentane mixture at 77 K. In case of the phenothiazine dioxide derivatives, the fluorescence and phosphorescence spectra were found to be well separated (Fig. 5 and Fig. S31, Table S5, ESI†) and the energy gap between the singlet and the triplet excited states resulting from these measurements was large (ΔE_{ST} *ca.* 0.6 eV, see Table S6, ESI†). A much smaller gap was observed for **NPI-Ph-PTZ**, with the ΔE_{ST} being *ca.* 0.17 eV (see Fig. 3 and Table S6, ESI†). Surprisingly, for **NPI-PTZ** and **NPI(3)-PTZ**, roughly overlapping fluorescence and phosphorescence spectra were recorded (Fig. 3 and Fig. S31, Table S5, ESI†), suggesting a negligible ΔE_{ST} in these cases (Table S6, ESI†).

These experimental results were found to be in good agreement with the theoretical TD-DFT predictions about the energies of the S_1 and T_1 excited states at their respective optimized geometries. Despite the fact that the absolute values of the singlet and triplet energies are sometimes not perfectly in line with the experimental findings, the obtained trend for the ΔE_{ST} among the molecules in the series is in excellent agreement (Table 4). It is noteworthy that the triplet energy is only slightly affected by changes in the molecular structure. On the other hand, the singlet energy shows important differences among the six compounds; the energy difference with respect to the T_1 state is much smaller for the oxygen-free derivatives, and particularly for **NPI-PTZ** and **NPI(3)-PTZ**, likely because of their increased ICT character (Fig. 6). The TD-DFT calculations also yield information about the structural and electronic features of the S_1 and T_1 states. The more significant structural rearrangement on passing from S_0 to S_1 for the PTZ relative to the PTZ(dioxy) derivatives (Fig. S41–S42, ESI†) is consistent with their relatively larger Stokes shift values experimentally measured (Table S1, ESI†). Additionally, while the S_1 usually exhibits an ICT nature being described by a HOMO localized on the PTZ/PTZ(dioxy) and a LUMO localized on the NPI, the T_1 is generally described by a configuration of NTOs localized on the NPI acceptor unit (Fig. 6 and Fig. S43, ESI†). This different orbital nature between S_1 (ICT) and T_1 (LE) is at the root of the significant spin-orbit coupling between the two states and thus of the efficient ISC experimentally observed for all these molecules. In summary, the ICT nature of the lowest excited singlet

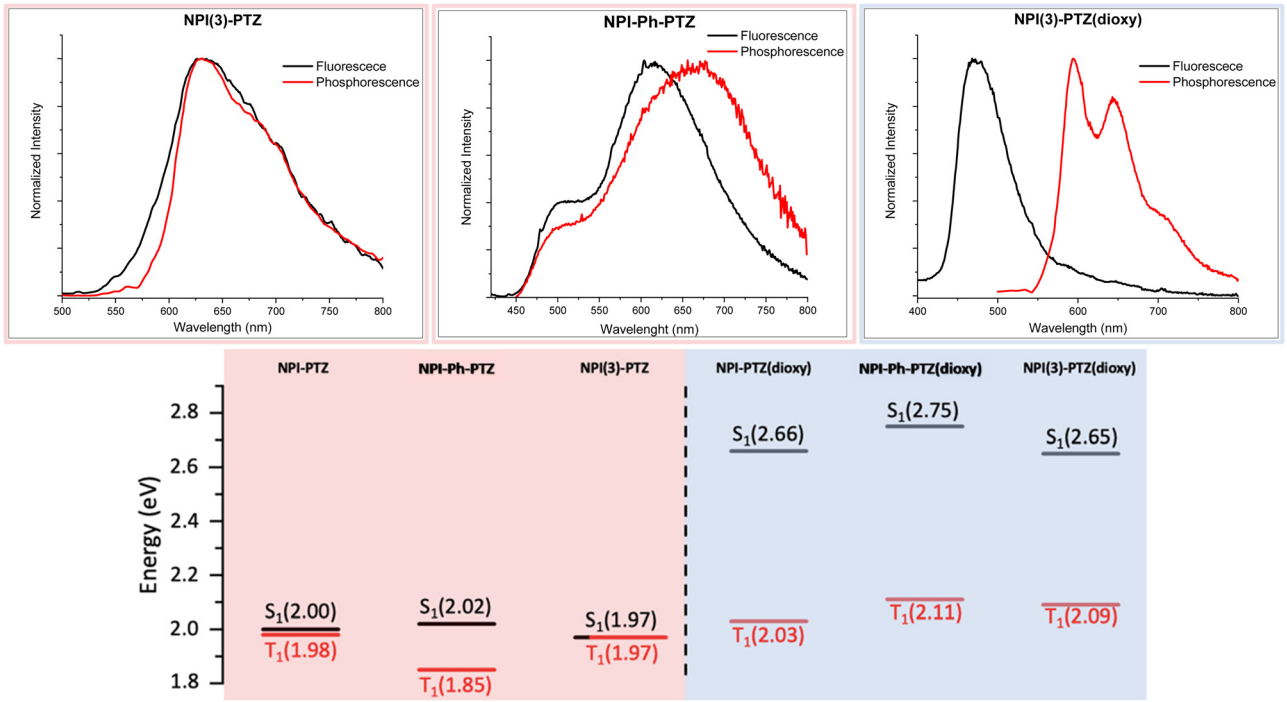

Fig. 5 Fluorescence and phosphorescence spectra in the mixture methylcyclohexane:3-methylpentane 9:1 (v/v) at 77K (upper graphs) together with the singlet and triplet energies of the investigated compounds obtained from these experiments (lower graphs).

Table 4 Predicted transitions from the lowest excited states (S_1 or T_1) in their relaxed geometry as obtained from the TD-DFT calculations

Molecule	Singlet emission (eV)	Triplet emission (eV)	ΔE_{ST} (eV)
NPI-PTZ	1.38	1.37	0.01
NPI-PTZ(dioxy)	2.43	1.47	0.96
NPI-Ph-PTZ	1.67	1.49	0.18
NPI-Ph-PTZ(dioxy)	2.79	1.48	1.31
NPI(3)-PTZ	1.56	1.46	0.10
NPI(3)-PTZ(dioxy)	2.39	1.48	0.91

state S_1 in these compounds makes it easily tunable in energy. This leads to the most significant energetic stabilization of the S_1 in the compounds showing the largest push–pull character (**NPI-PTZ** and **NPI(3)-PTZ**), with the lowest excited singlet state becoming isoenergetic to the triplet in these cases.[41]

Thermally activated delayed fluorescence

Given the negligible ΔE_{ST} demonstrated both experimentally and theoretically for **NPI-PTZ** and **NPI(3)-PTZ**, the possible occurrence of delayed fluorescence was attentively searched at room temperature for these molecules. The obtained results are reported in Fig. 7, in terms of fluorescence decay kinetics recorded by means of time correlated-single photon counting (TC-SPC) with nanosecond temporal resolution both in air-equilibrated and in nitrogen-purged toluene solution. The kinetics clearly exhibit a prompt decay component of few nanoseconds (2–8 ns), together with a delayed decay component characterized by lifetimes of tens/hundreds of nanoseconds in aerated solution which become significantly longer in de-aerated solution (Table 5). The lifetimes of this delayed emitting component are in perfect agreement with those obtained for the triplet excited state from the nanosecond transient absorption measurements (Table 5). Therefore, we have clear experimental evidence about the occurrence of delayed fluorescence for **NPI-PTZ** and **NPI(3)-PTZ** in toluene. No such evidence was found for the other investigated compounds, including **NPI-Ph-PTZ**, in agreement with their larger ΔE_{ST} which should disfavor the occurrence of r-ISC followed by delayed fluorescence. The determination of the fluorescence quantum yields in both air-equilibrated and nitrogen-purged conditions for **NPI(3)-PTZ** in toluene (Table S7, ESI†) allowed the r-ISC rate constant to be estimated according to a method of calculation reported in the literature by Adachi *et al.*[42] A value of 1.9×10^4 s^{-1} was obtained for the $k_{r\text{-}ISC}$ of **NPI(3)-PTZ** in toluene (see the details in the ESI†). This value is not exceptionally high but still higher than the limit considered necessary to be overcome in the literature for a material to be considered TADF-active.[43] The lower ϕ_F values of **NPI-PTZ** prevented an accurate estimate of the $k_{r\text{-}ISC}$ to be gained for this compound.

Aggregation-induced and solid-state delayed fluorescence

Given the low fluorescence efficiency observed for these fluorophores, particularly for the oxygen-free derivatives, and their structural flexibility as the donor and acceptor units are connected through single bonds, the possibility of an aggregation-induced emission behavior activated through restriction of intramolecular motions was considered and thoroughly investigated. To this aim, the absorption and emission properties of the compounds were studied in dimethylsulphoxide/water mixtures with different water fractions (see Fig. S32, S34 and Tables S8, S9, ESI†). Indeed, while

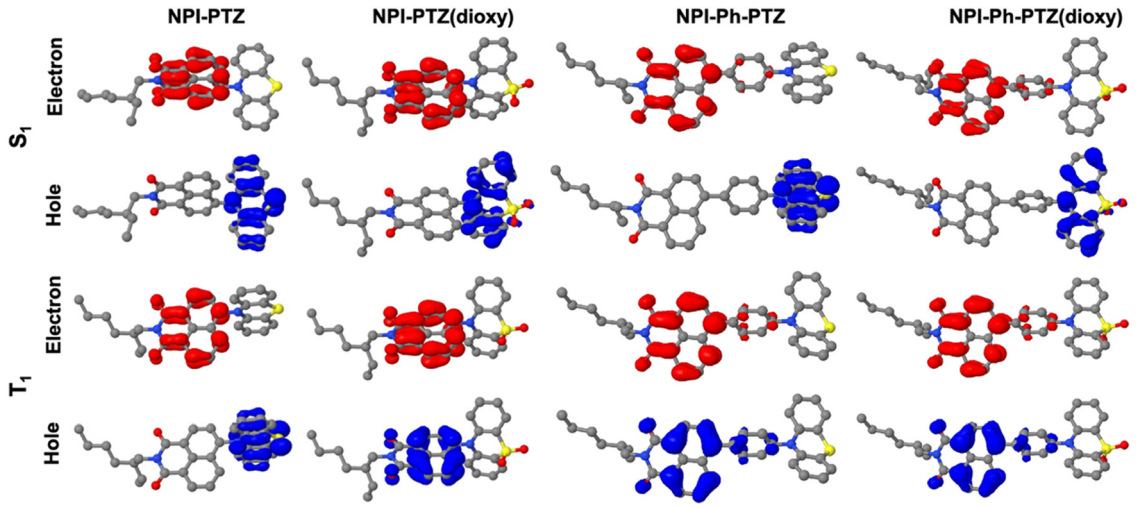

Fig. 6 Natural transition orbitals describing S_1 and T_1 in their optimized geometries as obtained from the TD-DFT calculations.

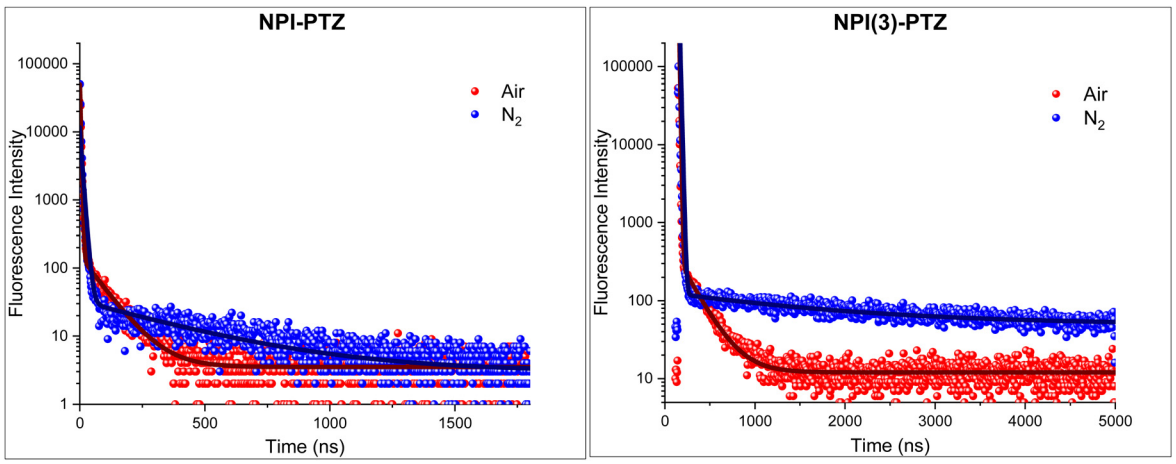

Fig. 7 Fluorescence decay kinetics of **NPI-PTZ** (left) and **NPI(3)-PTZ** (right) in air-equilibrated (red curve) and nitrogen-purged (blue curve) toluene together with their best fitting.

Table 5 Comparison between lifetimes of the compounds in air-equilibrated (air) and nitrogen-purged (N_2) toluene, obtained from the decay kinetics recorded with nanosecond transient absorption (TA) and single photon counting (SPC) techniques

	ns-TA		ns-SPC	
Compound	τ_{air} (ns)	τ_{N2} (ns)	τ_{air} (ns)	τ_{N2} (ns)
NPI-PTZ	6 (5%) 90 (95%)	6 (3%) 440 (97%)	2.4 (81%) 87 (19%)	3.5 (88%) 394 (12%)
NPI(3)-PTZ	5 (1%) 262 (99%)	19 (1%) 3400 (99%)	7.8 (89%) 215 (11%)	10 (87%) 1770 (13%)

dimethylsulphoxide is a good solvent for these organic fluorophores, water is a bad solvent and its increasing content in the mixtures leads to aggregate formation. Interestingly, aggregates were generally found to be more emissive than the corresponding monomers and were characterized by a bright blue emission for the phenothiazine dioxide derivatives and by red-emission for the phenothiazine derivatives, respectively (Fig. S33, ESI†). Strikingly, while the fluorescence decay of the monomer species took place in few/tens of nanoseconds in DMSO (see Tables S8 and S9, ESI†), the emission kinetics for the aggregates of the three oxygen-free phenothiazine derivatives in water dispersion were found to exhibit both a prompt and a delayed decay component (Fig. 8). The long emission of 392 ns, 1089 ns and 670 ns for **NPI-PTZ**, **NPI-Ph-PTZ** and **NPI(3)-PTZ**, respectively, is consistent with the occurrence of r-ISC from the triplet to the singlet followed by delayed fluorescence in the aggregates. We have thus evidence for aggregation-induced delayed fluorescence for these fluorophores.[23,44] It is particularly appealing that the TADF is enabled in the aggregates of **NPI-Ph-PTZ**, for which no such behavior was revealed in solution. This might be possibly associated to the stabilization of intermolecular charge transfer states in the aggregate species, as sometime discussed in the literature.[45]

Despite the quite low fluorescence quantum yields measured for the investigated compounds in solution, significant emissions were observed in the solid state. The emission of the phenothiazine dioxide derivatives in thin films obtained by spin-coating falls in the blue, while the emission of the

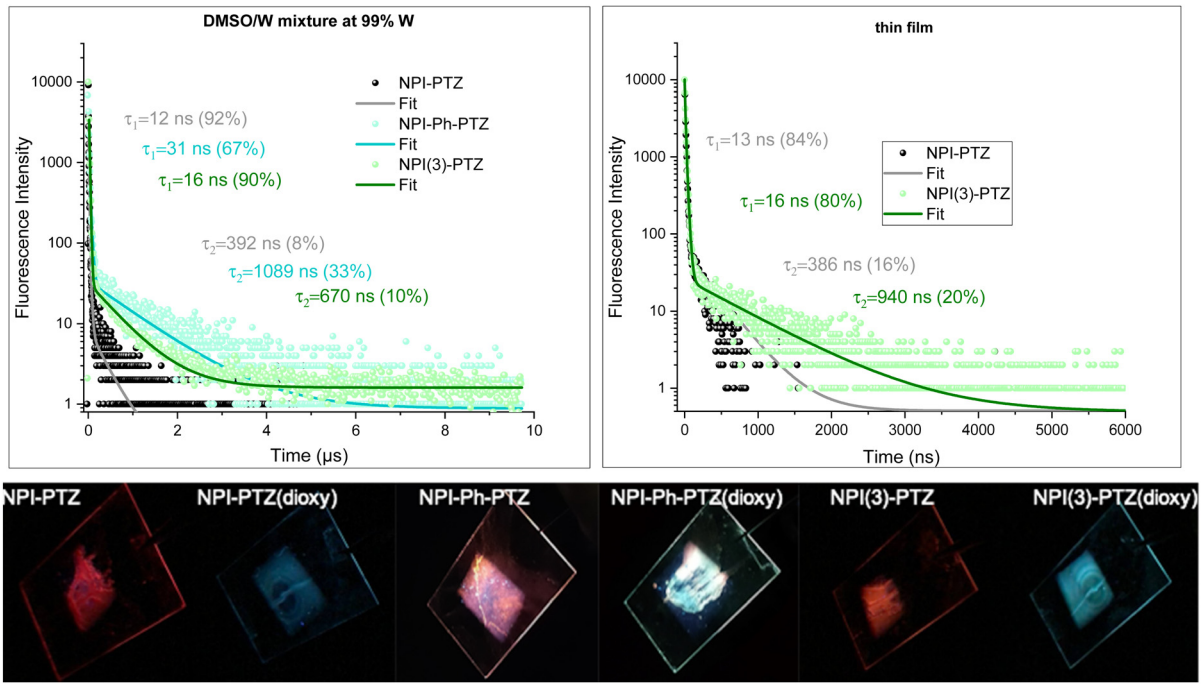

Fig. 8 (Upper panel) Fluorescence spectra decay kinetics of the investigated compounds in water dispersion (left) and in thin films (right) and relative fittings. (Lower panel) Photographs taken under UV-light of the film emission.

phenothiazine-based samples in the red (Fig. 8, Fig. S35 and Table S10, ESI†). This implies that the solid-state fluorescence of these organic materials is located in the two-extreme regions of the visible spectral range, the two regions rarely reached by employing the most common organic fluorophores. The TC-SPC measurements performed on the thin films of **NPI-PTZ** and **NPI(3)-PTZ** revealed in the fluorescence kinetics the presence of both a prompt component of tens of nanoseconds and a delayed component of hundreds of nanoseconds (Fig. 8). The observation of red TADF in the solid state for these new organic materials makes them very promising for applications in third generation OLED devices.

Conclusions

In this investigation, we report the synthesis of six new push–pull systems containing naphthalimide (NPI) as electron acceptor and phenothiazine/phenothiazine dioxide (PTZ/PTZ(dioxy)) as electron donors. The donor and acceptor units were arranged in dipolar (**NPI-PTZ** and **NPI-PTZ(dioxy)**) and octupolar (**NPI(3)-PTZ** and **NPI(3)-PTZ(dioxy)**) structures, and were connected not only by single bonds but also by a phenyl π-linker (**NPI-Ph-PTZ** and **NPI-Ph-PTZ(dioxy)**). This synthetic work was aimed at studying the effect of both tuning the push–pull strength and the molecular conjugation on the photobehaviour. The excited state dynamics, nature and energy of these chromophores were thoroughly investigated by means of an advanced joint spectroscopic and computational effort, involving time-resolved spectroscopies with both nanosecond and femtosecond temporal resolution as well as TD-DFT quantum chemical simulations. As a consequence of this mechanistic study, information about the structure-property relationships and the key factors necessary to activate red TADF in these materials was gained. Our time resolved spectroscopic and computational results showed that the increased push–pull character in the oxygen-free relative to the oxygen-functionalized phenothiazine derivatives was crucial to achieve negligible singlet-to-triplet energy splitting between the ICT S_1 and the LE T_1, and thus effective r-ISC and TADF. On the other hand, higher fluorescence efficiencies were obtained upon increasing the molecular conjugation by passing from dipolar to octupolar systems and particularly by introducing a phenyl spacer between the donor and the acceptor portions. Interestingly, intense red TADF was revealed and enhanced in aggregates of the phenothiazine-based fluorophores produced both in water dispersions and in thin films. The observation of red TADF in the solid state for these new organic materials makes them very promising for applications in third generation OLED devices.

Author contributions

C.M.: data curation, investigation, methodology, writing – review & editing; T.B.: data curation, investigation, methodology, writing – review & editing; M.S.: data curation, investigation, methodology, writing – review & editing; T.T.: data curation, investigation, methodology, writing – review & editing; G.C.: data curation, investigation, writing – review & editing; J.C.: investigation, supervision, writing – review & editing; R.M.: conceptualization,

supervision, writing – review & editing; B.C.: conceptualization, investigation, supervision, writing – original draft, writing – review & editing.

Conflicts of interest

There are no conflicts to declare.

Acknowledgements

CM, TB, GC and BC acknowledge support by the European Union – NextGenerationEU under the Italian Ministry of University and Research (MUR) National Innovation Ecosystem grant ECS00000041 - VITALITY - CUP J97G22000170005. JC acknowledges support from Le Fonds de la Recherche Scientifique (FNRS), Belgium.

Notes and references

1 Y. Liu, C. Li, Z. Ren, S. Yan and M. R. Bryce, *Nat. Rev. Mater.*, 2018, **3**, 1–20.
2 Y.-Z. Shi, H. Wu, K. Wang, J. Yu, X.-M. Ou and X.-H. Zhang, *Chem. Sci.*, 2022, **13**, 3625–3651.
3 M. Y. Wong and E. Zysman-Colman, *Adv. Mater.*, 2017, **29**, 1605444.
4 G. Hong, X. Gan, C. Leonhardt, Z. Zhang, J. Seibert, J. M. Busch and S. Bräse, *Adv. Mater.*, 2021, **33**, 2005630.
5 X. Cai and S.-J. Su, *Adv. Funct. Mater.*, 2018, **28**, 1802558.
6 T. Huang, X. Song, M. Cai, D. Zhang and L. Duan, *Mater. Today Energy*, 2021, **21**, 100705.
7 H. Tanaka, K. Shizu, H. Nakanotani and C. Adachi, *Chem. Mater.*, 2013, **25**, 3766–3771.
8 C. Chen, R. Huang, A. S. Batsanov, P. Pander, Y.-T. Hsu, Z. Chi, F. B. Dias and M. R. Bryce, *Angew. Chem.*, 2018, **130**, 16645–16649.
9 R. Ansari, W. Shao, S.-J. Yoon, J. Kim and J. Kieffer, *ACS Appl. Mater. Interfaces*, 2021, **13**, 28529–28537.
10 X.-K. Chen, D. Kim and J.-L. Brédas, *Acc. Chem. Res.*, 2018, **51**, 2215–2224.
11 F. B. Dias, T. J. Penfold and A. P. Monkman, *Methods Appl. Fluoresc.*, 2017, **5**, 012001.
12 H. Uoyama, K. Goushi, K. Shizu, H. Nomura and C. Adachi, *Nature*, 2012, **492**, 234–238.
13 D. H. Ahn, S. W. Kim, H. Lee, I. J. Ko, D. Karthik, J. Y. Lee and J. H. Kwon, *Nat. Photonics*, 2019, **13**, 540–546.
14 S. Kumar, P. Tourneur, J. R. Adsetts, M. Y. Wong, P. Rajamalli, D. Chen, R. Lazzaroni, P. Viville, D. B. Cordes, A. M. Z. Slawin, Y. Olivier, J. Cornil, Z. Ding and E. Zysman-Colman, *J. Mater. Chem. C*, 2022, **10**, 4646–4667.
15 Z. Cai, X. Wu, H. Liu, J. Guo, D. Yang, D. Ma, Z. Zhao and B. Z. Tang, *Angew. Chem., Int. Ed.*, 2021, **60**, 23635–23640.
16 U. Balijapalli, R. Nagata, N. Yamada, H. Nakanotani, M. Tanaka, A. D'Aléo, V. Placide, M. Mamada, Y. Tsuchiya and C. Adachi, *Angew. Chem., Int. Ed.*, 2021, **60**, 8477–8482.
17 D. Karthik, Y. H. Jung, H. Lee, S. Hwang, B.-M. Seo, J.-Y. Kim, C. W. Han and J. H. Kwon, *Adv. Mater.*, 2021, **33**, 2007724.
18 S. Kothavale, W. J. Chung and J. Y. Lee, *J. Mater. Chem. C*, 2021, **9**, 528–536.
19 U. Balijapalli, Y.-T. Lee, B. S. B. Karunathilaka, G. Tumen-Ulzii, M. Auffray, Y. Tsuchiya, H. Nakanotani and C. Adachi, *Angew. Chem., Int. Ed.*, 2021, **60**, 19364–19373.
20 M. Zhao, M. Li, W. Li, S. Du, Z. Chen, M. Luo, Y. Qiu, X. Lu, S. Yang, Z. Wang, J. Zhang, S.-J. Su and Z. Ge, *Angew. Chem.*, 2022, **134**, e202210687.
21 Y. Liu, X. Xiao, Y. Ran, Z. Bin and J. You, *Chem. Sci.*, 2021, **12**, 9408–9412.
22 S. Qi, S. Kim, V.-N. Nguyen, Y. Kim, G. Niu, G. Kim, S.-J. Kim, S. Park and J. Yoon, *ACS Appl. Mater. Interfaces*, 2020, **12**, 51293–51301.
23 J. Guo, Z. Zhao and B. Z. Tang, *Adv. Optic. Mater.*, 2018, **6**, 1800264.
24 R. Furue, T. Nishimoto, I. S. Park, J. Lee and T. Yasuda, *Angew. Chem., Int. Ed.*, 2016, **55**, 7171–7175.
25 X. Wang, S. Wang, J. Lv, S. Shao, L. Wang, X. Jing and F. Wang, *Chem. Sci.*, 2019, **10**, 2915–2923.
26 L. Wu, K. Wang, C. Wang, X.-C. Fan, Y.-Z. Shi, X. Zhang, S.-L. Zhang, J. Ye, C.-J. Zheng, Y.-Q. Li, J. Yu, X.-M. Ou and X.-H. Zhang, *Chem. Sci.*, 2021, **12**, 1495–1502.
27 M. Poddar, A. Cesaretti, E. Ferraguzzi, B. Carlotti and R. Misra, *J. Phys. Chem. C*, 2020, **124**, 17864–17878.
28 Y. Rout, A. Cesaretti, E. Ferraguzzi, B. Carlotti and R. Misra, *J. Phys. Chem. C*, 2020, **124**, 24631–24643.
29 Y. Rout, C. Montanari, E. Pasciucco, R. Misra and B. Carlotti, *J. Am. Chem. Soc.*, 2021, **143**, 9933–9943.
30 A. Cesaretti, T. Bianconi, M. Coccimiglio, N. Montegiove, Y. Rout, P. L. Gentili, R. Misra and B. Carlotti, *J. Phys. Chem. C*, 2022, **126**, 10429–10440.
31 G. Tang, A. A. Sukhanov, J. Zhao, W. Yang, Z. Wang, Q. Liu, V. K. Voronkova, M. Di Donato, D. Escudero and D. Jacquemin, *J. Phys. Chem. C*, 2019, **123**, 30171–30186.
32 M. Okazaki, Y. Takeda, P. Data, P. Pander, H. Higginbotham, A. P. Monkman and S. Minakata, *Chem. Sci*, 2017, **8**, 2677–2686.
33 R. Guo, Y. Wang, Z. Huang, Q. Zhang, S. Xiang, S. Ye, W. Liu and L. Wang, *J. Mater. Chem. C*, 2020, **8**, 3705–3714.
34 B. H. Jhun, D. Y. Jeong, S. Nah, S. Y. Park and Y. You, *J. Mater. Chem. C*, 2021, **9**, 7083–7093.
35 X. Li, S. Shen, C. Zhang, M. Liu, J. Lu and L. Zhu, *Sci. China Chem.*, 2021, **64**, 534–546.
36 B. Carlotti, A. Cesaretti, C. G. Fortuna, A. Spalletti and F. Elisei, *Phys. Chem. Chem. Phys.*, 2015, **17**, 1877–1882.
37 B. Carlotti, F. Elisei, U. Mazzucato and A. Spalletti, *Phys. Chem. Chem. Phys.*, 2015, **17**, 14740–14749.
38 E. Benassi, B. Carlotti, M. Segado, A. Cesaretti, A. Spalletti, F. Elisei and V. Barone, *J. Phys. Chem. B*, 2015, **119**, 6035–6040.

39 B. Carlotti, A. Spalletti, M. Šindler-Kulyk and F. Elisei, *Phys. Chem. Chem. Phys.*, 2011, **13**, 4519.
40 B. Carlotti, I. Kikaš, I. Škorić, A. Spalletti and F. Elisei, *ChemPhysChem*, 2013, **14**, 970–981.
41 L. Fisher, R. J. Vázquez, M. Howell, A. K. Muthike, M. E. Orr, H. Jiang, B. Dodgen, D. R. Lee, J. Y. Lee, P. Zimmerman and T. Goodson, *Chem. Mater.*, 2022, **34**, 2161–2175.
42 N. Notsuka, H. Nakanotani, H. Noda, K. Goushi and C. Adachi, *J. Phys. Chem. Lett.*, 2020, **11**, 562–566.
43 R. J. Vázquez, J. H. Yun, A. K. Muthike, M. Howell, H. Kim, I. K. Madu, T. Kim, P. Zimmerman, J. Y. Lee and T. G. Iii, *J. Am. Chem. Soc.*, 2020, **142**, 8074–8079.
44 B. Zhang, Y. Kong, H. Liu, B. Chen, B. Zhao, Y. Luo, L. Chen, Y. Zhang, D. Han, Z. Zhao, B. Z. Tang and L. Niu, *Chem. Sci.*, 2021, **12**, 13283–13291.
45 P. Tourneur, F. Lucas, C. Quinton, Y. Olivier, R. Lazzaroni, P. Viville, J. Cornil and C. Poriel, *J. Mater. Chem. C*, 2020, **8**, 14462–14468.